Macromolecules

pubs.acs.org/Macromolecules Article

Crystallization Kinetics of Crystalline−Crystalline and Crystalline−Amorphous Block Copolymers of Linear Polyethylene and Isotactic Polypropylene

Alessandra Cicolella, Miriam Scoti, Giovanni Talarico, Alejandro J. Müller, Rocco Di Girolamo,* and Claudio De Rosa*

Cite This: *Macromolecules* 2024, 57, 8748−8762 Read Online

ACCESS | Metrics & More | Article Recommendations | Supporting Information

ABSTRACT: Crystalline−amorphous diblock copolymers (BCPs) comprising crystalline blocks of isotactic polypropylene (iPP) or polyethylene (PE) linked to amorphous blocks of random ethylene−propylene copolymers (EPR) (iPP-*b*-EPR and PE-*b*-EPR) of different block lengths and ethylene concentrations in EPR blocks, and crystalline−crystalline BCPs composed by iPP and PE blocks (iPP-*b*-PE) have been synthesized with different living catalysts. The effects of the presence of a linked EPR rubbery block of varying composition on the crystallization behaviors and kinetics of PE and iPP, and of crystalline PE or iPP block on the crystallization kinetics of linked iPP or PE, respectively, have been analyzed. All samples have been isothermally crystallized from melting at different temperatures, and the crystallization kinetics have been analyzed. In iPP-*b*-PE BCPs, the PE block crystallizes first from the melt during nonisothermal cooling or isothermal crystallization. The iPP block crystallizes after PE and nucleates over the PE crystals. In both iPP-*b*-EPR and PE-*b*-EPR BCPs, the linked amorphous EPR block slows down the crystallization of iPP and PE blocks with respect to their respective homopolymers. Furthermore, in iPP-*b*-EPR samples, a higher concentration of propylene in the EPR phase results in a more significant slowdown of the crystallization kinetics of iPP due to a higher solubility between the blocks. Analogously, in PE-*b*-EPR copolymers, the increase in the length of the EPR block results in a more pronounced slowdown of the crystallization rate of PE with respect to the PE homopolymer due to the significant dilution exerted by the long EPR block. All samples of iPP-*b*-PE copolymers show crystallization rates lower than that of the PE homopolymer but faster than that of the iPP homopolymer. In isothermal crystallization experiments, the iPP blocks do not crystallize, not even at low crystallization temperatures, but crystallize upon successive cooling, nucleating over the PE crystals formed in the isothermal step. Therefore, the linked iPP, which remains in the melt during the isothermal crystallization, slows down the crystallization kinetics of PE, in contrast to what happens in a sample of iPP/PE blend, where the crystallization kinetics of PE is not affected by the presence of the phase-separated iPP.

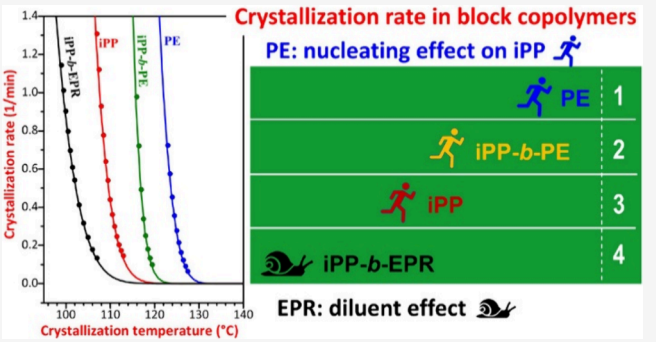

Downloaded via ECOLE POLYTECHNIC FED LAUSANNE on March 11, 2025 at 13:39:25 (UTC).
See https://pubs.acs.org/sharingguidelines for options on how to legitimately share published articles.

INTRODUCTION

Over the years, significant attention has been devoted to investigating the crystallization behavior of block copolymers (BCPs) containing one or two crystallizable segments, reflecting ongoing interest in this field.[1−11] It is widely recognized that the crystallization process of such materials is primarily affected by factors like molecular microstructure and architecture, molecular mass, number of crystallizable blocks, and crystallization conditions,[4−7,10−19] as well as segregation strength.[20−25] Crystallizable BCPs constituted by polymer blocks that are miscible in the melt or weakly segregated generally show solid-state morphologies dictated by the crystallization, as the first block that crystallizes upon cooling from the melt can form superstructures that template the crystallization of the other crystallizable block.[5,11,25−28] On the other hand, crystallizable BCPs that form phase-separated structures in the melt may exhibit confined crystallization within microdomains formed in the melt, giving different morphologies depending on composition and thermodynamic repulsion.[5,11,28−32] However, other phenomena may take place, as the breakout crystallization, where crystallization completely destroys the ordered structure of the melt, leading to the typical morphology of crystalline lamellae and spherulites,[5,11,17,33] or the pass-through crystallization where crystal-

Received: June 17, 2024
Revised: August 13, 2024
Accepted: August 30, 2024
Published: September 10, 2024

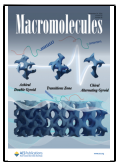

ACS Publications © 2024 American Chemical Society

line lamellae of one component growing inside microdomains pass through different microdomains without destroying the phase-separated structure.[5,11,19,34−42]

Several reports published in the last decades have convincingly demonstrated how the crystallization kinetics in BCPs are significantly influenced by confinement effects, miscibility, and also nucleation. For example, the nanoconfinement imposed by PE crystals in polyethylene-*block*-poly(ethylene oxide) (PE-*b*-PEO) BCPs produces a slower crystallization rate of the PEO block with respect to the same molecular weight PEO homopolymer.[30] Fractionated crystallization and "fractionated melting" further evidenced the strong confinement of the PEO block inside spherical microdomains.[30] In strongly segregated polyethylene-*block*-poly(L-lactide) (PE-*b*-PLLA) systems, the isothermal crystallization rate of the PLLA block decreases as compared to homo-PLLA by the covalently linked molten PE chains, as reported by Castillo et al.[31]

Decrease of the crystallization rates has also been observed in weakly segregated BCPs due to the miscibility between the blocks, as occurs in poly(L-lactide)-*block*-poly(caprolactone) (PLLA-*b*-PCL) BCPs, where the crystallization of the PLLA block is slowed down by a diluent effect exerted by the PCL block, which, in turn, crystallizes inside the interlamellar regions of the spherulites of PLLA formed before and give, for PCL contents lower than 40%, also in this case fractionated crystallization.[27] Moreover, Müller et al.[28] demonstrated that the crystallization rate of the PE block decreases to a larger extent when it is linked to a miscible ethylene−propylene block due to a strong diluent effect and to a lower extent by the confinement exerted by glassy PS, rubbery poly(D,L-lactide), and semicrystalline PLLA blocks. In the latter case, also the nucleation effect of PLLA crystals on PE must be considered in order to explain the lower crystallization kinetics of the PE block when covalently bonded to amorphous poly(D,L-lactide) rather than to the previously crystallized PLLA.[28]

The above-mentioned studies represent only a minority of the extensive literature published regarding block copolymer crystallization. However, despite the large number of papers published in this field, studies of the crystallization kinetics of monodisperse BCPs containing blocks of stereoregular isotactic polypropylene (iPP) are still missing. The crystallization kinetics of iPP have been studied only in the framework of physical blends,[43−52] which are systems under active investigation with the aim to improve their mechanical properties. Moreover, the studies concerning PE-based BCPs have been limited to systems containing blocks of highly defective PE segments obtained by hydrogenation of 1,4-polybutadiene blocks, therefore, containing significant fractions of 1-butene unit defects generated by hydrogenation of 1,2-polybutadiene unit defects present in the 1,4-polybutadiene block.[3,11,25,28,31]

Only in recent time the development of stereoselective catalysts has granted access to precise control over block length in living and stereoselective olefin polymerization,[53−60] thus, allowing the preparation of BCPs made of crystallizable blocks of stereoregular polypropylene and linear PE[17−19,59,60] and of PE-based BCPs with a melting temperature of the PE block higher than 120 °C.[61,62]

Here we report the analysis of the crystallization behavior and morphology of crystalline−crystalline BCPs in which iPP and linear PE blocks are linked (iPP-*b*-PE) and of crystalline−amorphous BCP samples in which an amorphous rubbery block of a random ethylene−propylene copolymer (EPR) is linked to a block of iPP (iPP-*b*-EPR) or a block of linear PE (PE-*b*-EPR). We describe for the first time how the crystallization behaviors of PE and iPP are affected by the presence of a linked EPR rubbery block of different block lengths and ethylene concentrations and the influence of a crystalline PE or iPP block on the crystallization kinetics of iPP or PE, respectively. The effects of the presence of covalently linked amorphous or crystalline blocks and of the strong or weak phase separation in the melt are compared. The comprehensive characterization of the crystallization behavior and kinetics of these novel materials is crucial to tuning their properties in pursuit of potential applications as compatibilizers in polymer blends or thermoplastic elastomers.

EXPERIMENTAL SECTION

Samples of crystalline−crystalline BCPs composed by iPP and PE blocks (iPP-*b*-PE) and samples of crystalline−amorphous BCPs comprising crystalline blocks of iPP or PE linked to an amorphous block of EPR (iPP-*b*-EPR and PE-*b*-EPR) were synthesized by living catalysis employing the catalytic systems shown in Chart 1.[59−62]

Chart 1. Hafnium (A) and Titanium (B) Complexes Used as Catalysts for the Preparation of the BCP Samples

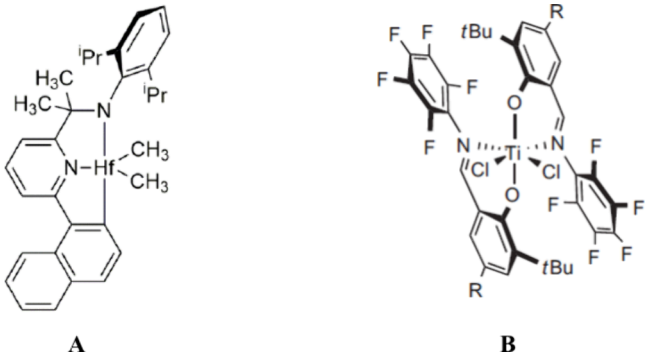

A B

The values of molecular mass, polydispersity, weight fractions of blocks, and ethylene concentrations in the EPR block of all the BCP samples are reported in Table 1. The samples are defined with the symbols iPP-PE-*x*, iPP-EPR-*x*-*z*, and PE-EPR-*y*-*z*, with *x* and *y* the weight fractions of iPP and PE blocks, respectively, and *z* the ethylene concentration in the EPR block (Table 1).

Samples of iPP homopolymer, iPP-*b*-PE, and iPP-*b*-EPR BCPs with blocks of different lengths were prepared using the pyridylamidohafnium complex and $B(C_6F_5)_3$ as catalytic system (Chart 1A), as reported in the Supporting Information.[59,60] The samples have total molar mass in the range of 113−180 kg/mol, several molar masses of the two blocks, and different ethylene concentrations in the EPR block.

PE homopolymer and PE-*b*-EPR BCPs samples were prepared by living polymerization using the organometallic catalyst based on the bis[*N*-(3-*tert*-butylsalicylidene)-2,3,4,5,6-pentafluoroanilinato]-titanium(IV) dichloride complex (Chart 1B), in combination with methylalumoxane (MAO), as reported in the Supporting Information.[61,62] The samples have total molar mass in the range of 67−140 kg/mol, different molar masses of the two blocks, and different ethylene concentrations in the EPR block.

Experimental details regarding the characterization by gel permeation chromatography (GPC), ^{13}C NMR, wide-angle X-ray diffraction, differential scanning calorimetry (DSC), polarized light optical microscopy (PLOM), and preparation of the blend of iPP and PE homopolymers are reported in the Supporting Information (SI).

The ^{13}C NMR spectra of the iPP homopolymer and of iPP-*b*-PE and iPP-*b*-EPR BCPs are reported in Figures S1−S3. The data

https://doi.org/10.1021/acs.macromol.4c01402
Macromolecules 2024, 57, 8748−8762

Table 1. Total Molecular Mass (M_n), Polydispersities (M_w/M_n), Molecular Masses of iPP, PE, and EPR Blocks and Concentration of Ethylene in the EPR Blocks of the iPP-*b*-PE, iPP-*b*-EPR, and PE-*b*-EPR BCPs

	M_n[a] (kDa)	M_w/M_n[a]	$M_{n(iPP)}$[a] (kDa)	$M_{n(PE)}$ (kDa)	$M_{n(EPR)}$ (kDa)	w_{iPP} (wt %)	w_{PE} (wt %)	$[E]$[d] (mol %)
iPP	139.8	1.29	139.8			100		
iPP-PE-64	180.6	1.26	94.6	86[b]		64[d]	36[f]	
iPP-PE-60	113.5	1.3	61.5	52[b]		60[d]	40[f]	
iPP-PE-52	163.5	1.19	64.6	98.9[b]		52[d]	48[f]	
iPP-EPR-38-43	178.2	1.17	67.8		110.4[b]	38[e]		43
iPP-EPR-40-29	161.2	1.26	64.4		96.8[b]	40[e]		29
PE	67.0	1.2		67.0[a]			100	
PE-EPR-69-76	87.7	1.27		60.8[a]	26.2[c]		69[g]	76
PE-EPR-45-62	139.9	1.44		63.3[a]	76.6[c]		45[g]	62

[a]From GPC. [b]From total M_n and $M_{n(iPP)}$, such as $M_{n(PE/EPR)} = M_n - M_{n(iPP)}$. [c]From total M_n and $M_{n(PE)}$, such as $M_{n(EPR)} = M_n - M_{n(PE)}$. [d]From ^{13}C NMR spectra. [e]From total M_n and $M_{n(iPP)}$, such as $w_{iPP} = M_{n(iPP)}/M_n$. [f]From w_{iPP}, such as $w_{PE} = 100 - w_{iPP}$. [g]From total M_n and $M_{n(PE)}$, such as $w_{PE} = M_{n(PE)}/M_n$.

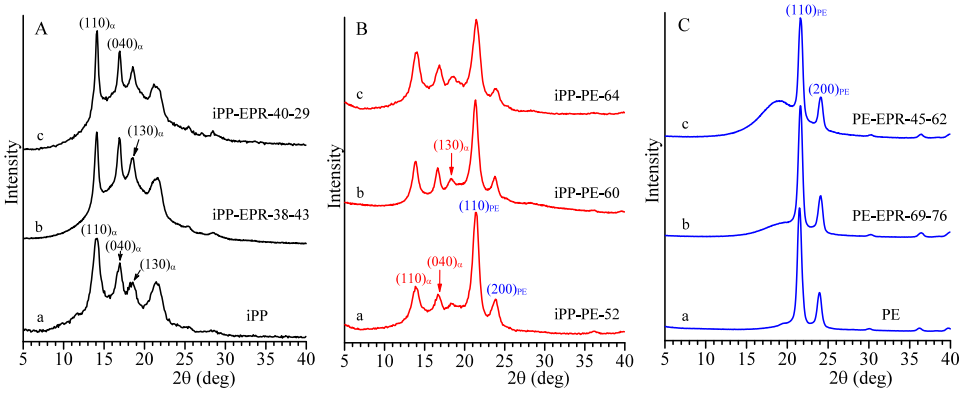

Figure 1. X-ray powder diffraction profiles of as-prepared samples of iPP-*b*-EPR (A), iPP-*b*-PE (B), and PE-*b*-EPR (C) BCPs and of iPP (profile a in part A) and PE (profile a in part C) homopolymers. The $(110)_\alpha$, $(040)_\alpha$, and $(130)_\alpha$ reflections at $2\theta = 14$, 17.1, and 18.6° of the α form of iPP and the $(110)_{PE}$ and $(200)_{PE}$ reflections at $2\theta = 21°$ and 24° of the orthorhombic form of PE are indicated.

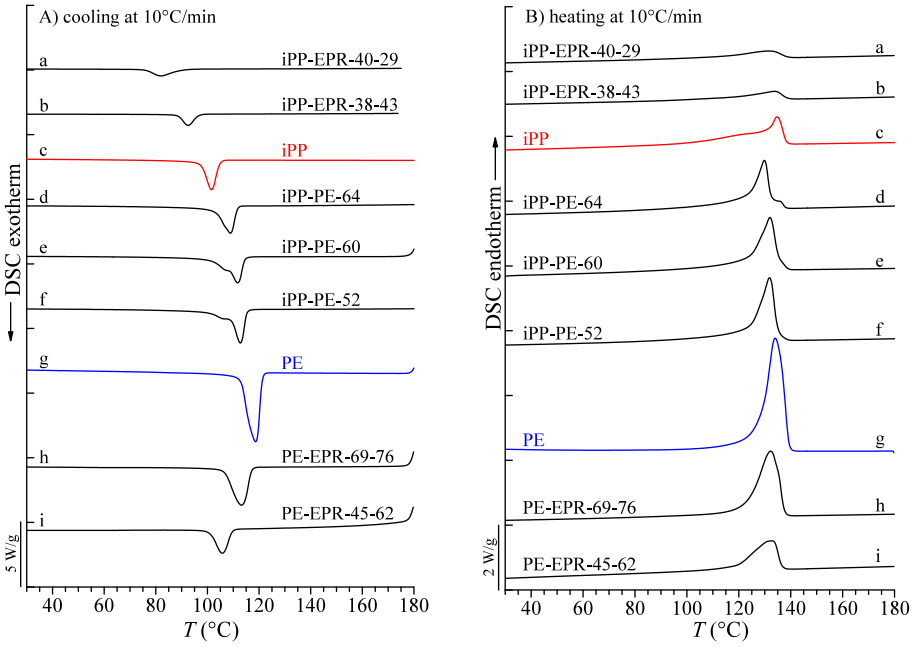

Figure 2. DSC curves recorded at 10 °C/min upon cooling from the melt (A) and successive heating of melt-crystallized samples (B) of iPP-*b*-EPR (a, b), iPP-*b*-PE (d–f), and PE-*b*-EPR (h, i) block copolymers and of iPP (c) and PE (g) homopolymers.

indicate that the iPP homopolymer and the iPP block within BCPs have moderate stereoregularity, with the concentration of the fully isotactic *mmmm* pentad being approximately 91%, and the presence of a significant amount of stereodefects represented by *rr* triads and about 2% of regiodefects due to 2,1 secondary propene units.[59] The ethylene content in EPR blocks of iPP-*b*-EPR was evaluated from the

https://doi.org/10.1021/acs.macromol.4c01402
Macromolecules 2024, 57, 8748−8762

Table 2. Crystallization Temperature and Enthalpy (T_c and ΔH_c), Melting Temperature and Enthalpy (T_m and ΔH_m) of iPP and PE Homopolymers, and iPP-*b*-EPR, iPP-*b*-PE, and PE-*b*-EPR BCPs with w_{iPP} and w_{PE} Weight Fractions of iPP and PE Blocks, Respectively, and [*E*] the Ethylene Concentrations in the EPR Block, and Glass Transition Temperature (T_g) of iPP-*b*-EPR and PE-*b*-EPR BCPs

sample	w_{iPP} (%)	w_{PE} (%)	[*E*] (mol %)	T_c[a] (°C)	ΔH_c (J/g)	T_m[b] (°C)	ΔH_m (J/g)	T_g[c] (°C)
iPP	100			102.0	77	134.7	−77	−11.5
iPP-EPR-40-29	40		29	81.9	32	131.4	−30	−33.6
iPP-EPR-38-43	38		43	92.5	30	133.7	−30	−42.3
iPP-PE-64	64	36		109.2	89	130.0; 136.8	−92	
iPP-PE-60	60	40		107.4; 111.7	90	132.0	−103	
iPP-PE-52	52	48		106.0; 112.6	110	131.9	−114	
PE		100		118.5	198	134.0	−193	
PE-EPR-69-76		69	76	113.2	136	132.3	−138	−52.7
PE-EPR-45-62		45	62	105.8	70	132.7	−69	−53.0

[a]From the DSC cooling scans of Figure 2A. [b]From the DSC heating scans of Figure 2B. [c]From the DSC heating scans of Figures S5 and S6.

integration of selected resonances of the ^{13}C NMR spectra reported in Figure S3, SI. The ^{13}C NMR spectra of PE-*b*-EPR BCPs are reported in Figure S4. The propene concentration in the EPR block was estimated from the ^{13}C NMR spectra of Figure S4, SI.

RESULTS AND DISCUSSION

X-ray Diffraction. The X-ray powder diffraction profiles of as-prepared samples of iPP and PE homopolymers and iPP-*b*-PE, iPP-*b*-EPR, and PE-*b*-EPR BCPs are reported in Figure 1. The iPP homopolymer (profile a of Figure 1A) and the iPP blocks within the iPP-*b*-EPR (profiles b and c of Figure 1A) and iPP-*b*-PE (profiles a−c of Figure 1B) BCPs are crystallized in the α form of iPP, as indicated by the presence of $(110)_\alpha$, $(040)_\alpha$, and $(130)_\alpha$ reflections at 2θ = 14, 17, and 18.6°, respectively,[63,64] in the diffraction profiles of Figure 1A,B.

The PE homopolymer (profile a of Figure 1C) and the PE blocks in the iPP-*b*-PE (profiles a−c of Figure 1B) and PE-*b*-EPR (profiles b and c of Figure 1C) BCPs are crystallized in the stable orthorhombic form of PE, as indicated by the presence of $(110)_{PE}$ and $(200)_{PE}$ reflections at 2θ = 21° and 24°, respectively,[65] in the diffraction profiles of Figures 1B,C. However, in both iPP-*b*-EPR and PE-*b*-EPR BCPs, the crystalline reflections overlap with the amorphous halo of EPR blocks, and the decrease of PE weight fraction in PE-*b*-EPR samples from 69 to 45 wt % (profiles b and c of Figure 1C) results in a crystallinity decrease.

In samples of iPP-*b*-PE, the concurrent presence of the reflections of PE and iPP crystals are clearly visible in the diffraction profiles of Figure 1B, and the increase of the fractional amount of PE crystals with decreasing the iPP block length is clearly indicated by the intensity increase of the $(110)_{PE}$ and $(200)_{PE}$ reflections of PE with decreasing iPP weight fraction.

Nonisothermal Crystallization. The DSC curves recorded at 10 °C/min upon cooling from the melt and successive heating of all BCP samples are reported in Figure 2. The crystallization and melting temperatures are listed in Table 2. From the DSC cooling scans in Figure 2A, it is clear that the crystallization behavior of iPP and PE blocks in the BCPs is significantly affected by the linked amorphous or crystalline blocks. The iPP and PE homopolymers (curves c and g of Figure 2A) crystallize at 102.0 and 118.6 °C, respectively, whereas the peak crystallization temperatures (T_c) of the iPP and PE blocks in the crystalline−amorphous iPP-*b*-EPR and PE-*b*-EPR BCPs samples (curves a, b, h, i of Figure 2A) are considerably lower than those of the iPP and PE homopolymers, due to the partially miscible linked amorphous EPR block.

The two iPP-*b*-EPR copolymers have similar weight fractions of the iPP blocks but crystallize at crystallization temperatures different by ≈10 °C (curves a and b of Figure 2A) that should be ascribed to the different ethylene concentrations in the EPR block. In fact, the lower T_c shown by the sample iPP-EPR-40-29 ([*E*] = 29 mol %) compared to the sample iPP-EPR-38-43 ([*E*] = 43 mol %) could be explained by the lower ethylene concentration in the EPR phase and, therefore, by a higher solubility between EPR and iPP blocks. The two PE-*b*-EPR samples (curves h, i of Figure 2A) are characterized by different lengths of the PE blocks and different ethylene concentrations in the EPR blocks, and the length of the PE block seems to have the decisive role. In fact, the sample PE-EPR-45-62 with a lower PE length and lower ethylene concentration in the EPR block, which could result in a less soluble amorphous block, shows lower T_c with respect to samples PE-EPR-69-76 due to higher dilution exerted by the longer EPR block.

In the case of the double crystalline iPP-*b*-PE copolymers, the presence of a broad exothermic phenomenon in the DSC cooling scans (curves d−f of Figure 2A) indicates that the two blocks crystallize in the same temperature range. This is due to the moderate stereoregularity of iPP homopolymer and of the iPP blocks produced by the catalyst A of Chart 1, and consequent low crystallization and melting temperatures of iPP, approaching those of PE (Table 2).[17,18] A similar single exothermic peak has also been observed in the cooling scans of iPP-*b*-PE polydisperse block copolymers obtained by techniques of chain shuttling polymerization.[66] However, the PE homopolymer crystallizes at 118 °C, whereas the iPP homopolymer crystallizes at lower temperature of 102 °C (curves c and g of Figure 2A), and the iPP-*b*-PE BCPs crystallize at temperatures higher than the iPP homopolymer, approaching that of the PE homopolymer with the increase of the PE block length (curves d−f of Figure 2A and Table 2). This suggests that the PE blocks crystallize first by cooling from the melt, and the iPP blocks crystallize at slightly lower temperatures and nucleate on the previously formed crystals of PE.[17,18] In particular, the DSC cooling curves of the samples iPP-PE-60 and iPP-PE-52 with the shortest iPP blocks (curves e, f of Figure 2A) show an intense exothermic peak that could correspond to the crystallization of PE block, and a shoulder at lower temperature presumably due to the crystallization of iPP. The crystallization behavior of our iPP-*b*-PE samples differs

https://doi.org/10.1021/acs.macromol.4c01402
Macromolecules 2024, 57, 8748−8762

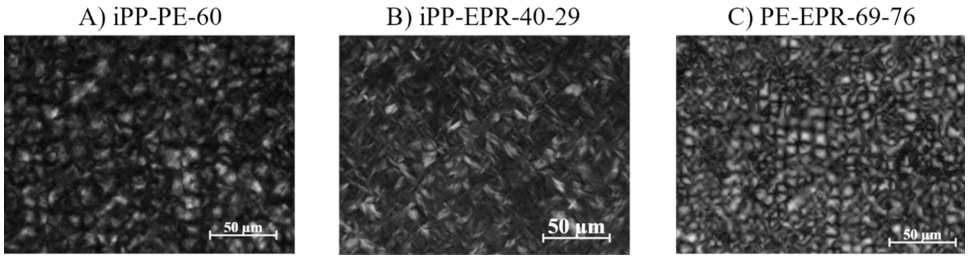

Figure 3. PLOM images recorded at 25 °C after crystallization from the melt by cooling at 10 °C/min of BCP samples iPP-PE-60 with w_{iPP} = 60% (A), iPP-EPR-40-29 with w_{iPP} = 40% and [E] = 29 mol % (B), and PE-EPR-69-76 with w_{PE} = 69% and [E] = 76 mol % (C).

from that shown by iPP/PE blends in which highly isotactic iPP crystallizes at nearly 130 °C, followed by the crystallization of PE at lower temperatures.[50,51]

The DSC melting scans of the samples crystallized from the melt are reported in Figure 2B. As mentioned above, the iPP homopolymer (curve (c) of Figure 2B) melts at a low temperature of nearly 135 °C, similar to the melting temperature of the PE homopolymer (curve (g) of Figure 2B), consistent with the moderate stereoregularity. The broad melting endotherm of the iPP homopolymer with a shoulder of the main peak at low temperature (curve (c) of Figure 2B) indicates crystallization of iPP from the melt in mixtures of α and γ forms, according to the moderate stereoregularity of the sample.[63,64] It is, indeed, well-known that defective iPPs and copolymers of iPP tend to crystallize in the γ form in mixture with the α form and the amount of γ form increases with increasing concentration of defects (stereodefects and comonomeric units).[63,67−82] This is demonstrated by the X-ray diffraction profiles of the iPP sample crystallized by cooling from the melt (as in Figure 2) reported in Figure S27 of the SI, showing the $(110)_\alpha$, $(040)_\alpha$ and $(130)_\alpha$ reflections at 2θ = 14, 17.1 and 18.6° of the α form of iPP and the $(117)_\gamma$ reflection of the γ form at 2θ = 20.1° (profile b of Figure S27).

All BCPs samples melt at temperatures only slightly lower than those of the homopolymers. This indicates that in crystalline−amorphous copolymers, the linked EPR block does not seem to affect much the melting behavior of the crystalline iPP or PE blocks. The DSC heating scans starting from lower temperatures in Figures S5 and S6 show that the glass transition temperature decreases with increasing ethylene concentration in iPP-*b*-EPR samples, and a more evident inflection is present in PE-*b*-EPR copolymers when increasing the EPR block length. Finally, in the iPP-*b*-PE samples, the presence of a single broad endothermic peak in the heating scans (curves d−f of Figure 2B) indicates a simultaneous melting of the two blocks. Only the sample iPP-PE-64 with the iPP block of highest molar mass (curve d of Figure 2B) presents a main peak at 130 °C and an additional shoulder at higher temperature (≈136 °C), probably due to the melting of iPP block crystals.

Bulk Morphology. The PLOM images recorded at room temperature on films of selected BCPs slowly crystallized from the melt are shown in Figure 3. The images of the iPP and PE homopolymers and of the other BCP samples are reported in Figure S7 of the SI. The iPP homopolymer (Figure S7A) shows the typical morphology of stereodefective iPPs, in which crystals of α and γ forms can coexist, characterized by small bundles of lamellae arranged in an almost 90° texture.[83,84] The PE homopolymer features instead small banded spherulites (Figure S7B), which are common in PE samples.[85−89] Banding is commonly attributed to the twist of radiating crystalline lamellae, although alternative views can also be found in the literature.[85−89]

The BCP sample iPP-PE-60 (Figure 3A) shows a morphology that seems to be defined uniquely by the crystallization of banded spherulites of the PE block, confirming that this block crystallizes first, and crystallization of the iPP block should then occur inside the preformed spherulites in a templated fashion.

It is worth mentioning that in the melt of iPP-*b*-PE BCPs the two immiscible iPP and PE give phase separation with formation of a microdomain structure that has been revealed by transmission electron microscopy (TEM) of samples rapidly crystallized from the melt by quenching in liquid nitrogen.[17] The rapid quenching prevents crystallization of the α form of iPP and only small PE crystals form resulting in preservation of the melt morphology that can be revealed at room temperature by TEM.[17] The incompatibility and phase-separation of iPP and PE in the melt found in our iPP-*b*-PE BCPs is well described in literature for immiscible iPP/HDPE blends that present unstable melt morphology and interaction parameter χ at temperatures of the melt (170−180 °C) in the range of 0.03−0.10,[90] leading to various phase-separated morphologies depending on the component viscosity ratio.[90−100] It is also well-known that this phase-separation leads to brittle and poor materials due to low interfacial adhesion.[101−104]

Considering that the total molecular weight of our samples is in the range 110−180 kg/mol (Table 1), the number of total equivalent segments N of the chains of the BCPs (one segment is four methylene carbon atoms) is in the range 2000−3200 ($N = M_n/56$, where 56 is the molecular mass of the segment of the BCP). Assuming the same values of the interaction parameter χ of 0.03−0.10 for our iPP-*b*-PE BCPs at the temperature of the melt (170−180 °C), values of the product χN much higher than 10 result and, therefore, a strong phase separation in the melt is expected for all samples of iPP-*b*-PE BCPs.[17,18]

The PLOM image in Figure 3A of the sample iPP-PE-60 suggests that the slow crystallization of iPP-*b*-PE BCPs destroys the expected phase-separated microstructure present in the melt. The PLOM images of samples of iPP-*b*-EPR (Figure 3B) and PE-*b*-EPR (Figure 3C) BCPs show the typical morphologies of the homopolymers, that is, bundles of lamellae in iPP-*b*-EPR (Figure 3B) and banded spherulites in PE-*b*-EPR (Figure 3C), as expected for melt miscible crystalline−amorphous BCPs. The different ethylene concentrations in the EPR blocks do not seem to affect the morphology.

Another observation that can be made regarding the superstructural morphology shown in Figure 3, is that the semicrystalline aggregates have relatively similar sizes, indicat-

https://doi.org/10.1021/acs.macromol.4c01402
Macromolecules 2024, 57, 8748−8762

ing a primary nucleation process that should be close to instantaneous.

Overall Crystallization Kinetics. All iPP-*b*-PE, iPP-*b*-EPR, and PE-*b*-EPR BCPs samples have been isothermally crystallized from the melt at different crystallization temperatures (T_c) to analyze the influence of the covalently linked amorphous or crystalline blocks on the overall crystallization kinetics of iPP and PE. Moreover, samples of blends of iPP and PE have also been analyzed to compare the crystallization kinetics of iPP and PE in phase-separated blends with the crystallization kinetics of the same components when they are linked in the iPP-*b*-PE BCPs. The isothermal crystallization experiments were performed by DSC, as described in the SI.[105] The obtained data were analyzed with Avrami's model[106,107] and Lauritzen and Hoffman's (L−H) theory.[108,109] The experimental data were fitted with the mentioned theories using the free Origin App developed by Müller et al.[105,110]

The DSC crystallization exotherms recorded during isothermal crystallization at different temperatures and the subsequent DSC heating curves of the melt-crystallized samples starting from the crystallization temperature are reported in Figures S8−S16 of the SI. The data for the iPP and PE homopolymers (Figures S8 and S9) are compared with those of the iPP-*b*-EPR (Figures S10 and S11), PE-*b*-EPR (Figures S12 and S13) and iPP-*b*-PE (Figures S14−S16) BCPs. The equilibrium melting temperatures (T_m^0) of the homopolymers and all block copolymer samples have been evaluated from the experimental melting temperatures (T_m) of the melt-crystallized samples with the Hoffman−Weeks extrapolation in the plots of the melting temperature as a function of the crystallization temperature.[111] The melting temperatures of the melt-crystallized samples were determined from the DSC heating curves as those in Figures S8B−S16B but in other independent experiments. In fact, in order to avoid lamellar thickening during the isotherms, the melting temperatures after the isothermal crystallization at each T_c were determined in other experiments in which the samples were not crystallized completely, but were crystallized until a time corresponding to the peak of the crystallization exotherm of Figures S8A−S16A ($t_c = t_p$). The obtained extrapolated values of T_m^0 are reported in Table S3 of the SI.

From the isothermal crystallization curves in Figures S8A−S16A, the induction time t_0, that is, the incubation time that elapses before any crystallization starts and during which primary nucleation takes place, has been determined for each crystallization temperature T_c. The inverse of the induction time $1/t_0$ is proportional to the primary nucleation rate before the growth starts.

The apparent crystallinity, that is, the weight fraction W_c of the crystallizable material crystallized at the time t, has been evaluated from the partial crystallization enthalpies of the isothermal crystallization exotherms of Figure S8A−S16A as $W_c(t) = \Delta H_c(t)/\Delta H_c(\text{total})$. The increase of the apparent crystallinity W_c with the crystallization time is shown in the kinetic curves of Figure S17, for iPP and PE homopolymers, Figure S18 for iPP-*b*-EPR BCPs, Figure S19 for PE-*b*-EPR and Figure S20 for iPP-*b*-PE BCPs.

The values of half-crystallization time $\tau_{50\%}$, which represents the time needed for 50% of the crystallizable material to nucleate and grow (i.e., overall crystallization), have been evaluated from the kinetic curves of Figures S17−S20. The inverse of half-crystallization time $1/\tau_{50\%}$ gives the experimental overall crystallization rate that includes contributions of both nucleation and growth.

The obtained experimental values of the induction time t_0, nucleation rate $1/t_0$, half crystallization time $\tau_{50\%}$ and crystallization rate $1/\tau_{50\%}$, along with the crystallization rate constant K and Avrami index n obtained by the fitting to Avrami's equation, are reported in Tables S4−S12 of the SI. The values of Avrami parameters n and $K^{1/n}$ are plotted as a function of T_c in Figure S21. The trends of the Avrami constant $K^{1/n}$ are very similar to those of the experimental values of $1/\tau_{50\%}$ reported below and in Figure S22, attesting to the good fit of the Avrami model. The values of the Avrami index (Figure S21A) fluctuate from 2 to 3. A value of $n = 2$ corresponds to two-dimensional growth and instantaneous nucleation. The value of $n = 3$ could be due to two-dimensional growth and sporadic nucleation or three-dimensional growth (spherulites) and instantaneous nucleation. The increase in Avrami index that can be observed with T_c for most samples indicates that nucleation tends to change from instantaneous to sporadic as the temperature increases. The results of the L−H fitting are reported in Table S13. All data reported in the SI are discussed below separately for crystalline−amorphous iPP-*b*-EPR and PE-*b*-EPR BCPs and crystalline−crystalline iPP-*b*-PE samples.

Crystalline−Amorphous BCPs. The values of the melting temperatures of isothermally crystallized samples of iPP and PE homopolymers and of iPP-*b*-EPR and PE-*b*-EPR BCPs, evaluated as described above and in SI, are reported in the Hoffman−Weeks plot of Figure 4 as a function of the crystallization temperature. The values of the equilibrium melting temperature T_m^0 estimated by the Hoffman−Weeks extrapolations of Figure 4 are shown in Table S3.

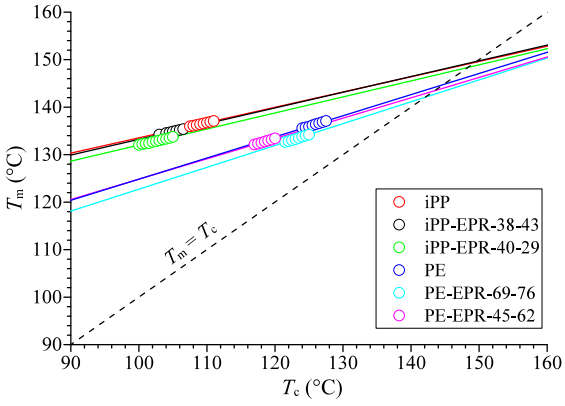

Figure 4. Hoffmann−Weeks linear fit of melting temperatures (T_m) as a function of the crystallization temperature (T_c) for the iPP and PE homopolymers and for the iPP-*b*-EPR and PE-*b*-EPR block copolymers.

In the case of the iPP homopolymer (Figure S8), the melting endotherms of the samples isothermally crystallized at different temperatures show two melting peaks at any crystallization temperature, and the enthalpy of the peak at low temperature increases with increasing crystallization temperature. As discussed above for the case of the samples crystallized by cooling from the melt of Figure 2, defective iPPs crystallize from the melt even in isothermal conditions in mixtures of α and γ forms and the amount of γ form, generally, increases with increasing crystallization temperature.[67−70,74,80−82] This is demonstrated by the X-ray diffraction

https://doi.org/10.1021/acs.macromol.4c01402
Macromolecules 2024, 57, 8748−8762

profiles of some iPP samples isothermally crystallized from the melt reported in Figure S27 of the SI that present the $(110)_\alpha$, $(040)_\alpha$, and $(130)_\alpha$ reflections at 2θ = 14, 17.1, and 18.6° of the α form of iPP and the $(117)_\gamma$ reflection of the γ form at 2θ = 20.1° (profiles c and d of Figure S27). Moreover, Figure S27 shows that the intensity of the $(117)_\gamma$ reflection of the γ form increases in melt-crystallized samples compared to the as-prepared sample and increases with increasing crystallization temperature, indicating an increase of the amount of γ form that crystallizes from the melt with increasing crystallization temperature. Therefore, the two melting peaks in the DSC curves of Figure S8B correspond to the melting of crystals of the γ form, at low temperature, and of the α form, at high temperature, formed in the isothermal crystallizations,[70,74,79−82] as confirmed by the increase of the enthalpy of the low temperature peak with increasing crystallization temperature.[67−70,74,80−82]

Since the α form is the most common and stable polymorphic modification of iPP,[64] we have used the higher melting temperature peak of the α form in the Hoffman−Weeks plot of Figure 4 to evaluate the extrapolated equilibrium melting temperature of this defective sample of iPP. The obtained value of T_m^0 = 149.9 °C for the neat iPP is considerably lower than the equilibrium melting temperature of 186.1 °C of iPP reported in the literature.[112−120] This can be explained by the moderate stereoregularity of our iPP sample prepared with catalyst A of Chart 1. The obtained value is, indeed, similar to the value of T_m^0 found for samples of iPP of similar isotacticity prepared with metallocene catalysts[121] (see Table 1 of ref 121). The data of Figure 4 indicate that the extrapolated equilibrium melting temperatures of the two samples of iPP-*b*-EPR BCPs are very similar to those of the iPP homopolymer, regardless of the length of the EPR block and of the ethylene concentration in the EPR block, indicating a stereoregularity of the iPP block similar to that of the homopolymer. Similarly, the extrapolated values of T_m^0 for the PE-*b*-EPR samples (Table S3) are very close to that of the PE homopolymer (144.7 °C). These data indicate that the linked amorphous block does not affect the value of the equilibrium melting temperature of the crystalline iPP or PE blocks.

Figure 5 shows the inverse of the induction time $(1/t_0)$, which is proportional to the primary nucleation rate before the beginning of the crystallization, as a function of the crystallization temperature for the iPP and PE homopolymers and for the iPP-*b*-EPR and PE-*b*-EPR BCPs. It is apparent that if the curves are extrapolated to be compared at the same values of T_c, PE nucleates faster than iPP and the crystalline blocks of iPP-*b*-EPR and PE-*b*-EPR show a lower nucleation rate compared to the corresponding homopolymers.

The values of the inverse of the half crystallization time $(1/\tau_{50\%})$, which represents the overall crystallization rate, are plotted in Figure 6 as a function of T_c (Figure 6A) and of the supercooling $\Delta T = T_m^0 - T_c$ (Figure 6B), calculated from the equilibrium melting temperatures T_m^0 of Table S3. The data of the overall crystallization rate have also been fitted with the Lauritzen and Hoffman (L−H) theory, assuming crystallization in Regime II, according to the literature.[115,122] Regime II is indeed assumed for the crystallization of iPP samples when the undercooling is between 37 and 48 °C,[115,122] and for PE samples crystallized with undercoolings higher than 17 °C.[123] More details regarding the choice of the parameters for the fitting are reported in SI.

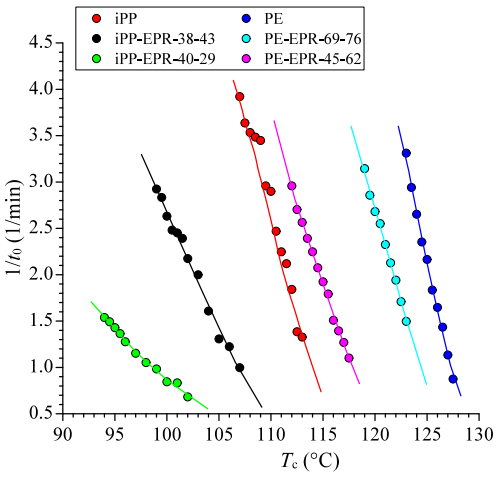

Figure 5. Inverse of the induction time $(1/t_0)$ as a function of the isothermal crystallization temperature T_c for the iPP and PE homopolymers and for the iPP-*b*-EPR and PE-*b*-EPR BCPs.

The trend of the overall crystallization rate of Figure 6 is similar to that of the nucleation rate of Figure 5, probably indicating that the primary nucleation process makes an important contribution to the overall crystallization kinetics.

The data of Figure 6 indicate that both iPP-*b*-EPR and PE-*b*-EPR copolymers exhibit overall crystallization rates lower than those of the corresponding homopolymers. Therefore, the presence of the amorphous EPR block clearly slows the overall crystallization of the attached miscible crystallizable block through a diluent effect. Moreover, since the two samples of iPP-*b*-EPR BCPs are characterized essentially by the same weight fraction of the iPP block (38 wt % in iPP-EPR-38-43 and 40 wt % in iPP-EPR-40-29), the lower crystallization rate of the sample iPP-EPR-40-29 can be explained uniquely by the lower concentration of ethylene in the EPR block (29% against 43%). As already discussed to explain the lower crystallization temperature of the sample iPP-EPR-40-29 upon cooling from the melt, the lower ethylene concentration of this sample results in an EPR block that is more miscible with the iPP block and, thus, more capable of affecting its crystallization kinetics through an improved diluent effect. For PE-*b*-EPR samples, the data of Figure 6 show that the sample PE-EPR-45-62 with the shortest PE block (w_{PE} = 45 wt %) shows the most pronounced slowdown of the crystallization rate with respect to the PE homopolymer owing to the strong dilution effect exerted by the longer EPR block.

Crystalline−Crystalline BCPs. The DSC data of Figure 2A have suggested that in the samples of iPP-*b*-PE BCP (curves d−f of Figure 2A), the PE block crystallizes first at a higher temperature upon cooling, and the iPP blocks crystallize at a slightly lower temperature and nucleate over the PE crystals formed before.[17,18] This has been demonstrated by simultaneous time and temperature resolved wide-angle diffraction and small-angle scattering measurements during cooling from the melt,[18] and here confirmed by the PLOM analysis (Figures 3 and S7). However, the single broad peak in the DSC heating curves of the melt-crystallized samples (curves d−f of Figure 2B), indicating melting of the iPP and PE blocks at nearly the same temperature, does not allow discrimination of whether crystallization of both iPP and PE has occurred. Only the sample iPP-PE-64 with the iPP block of highest molar mass (curve d of Figure 2B) presents a shoulder

https://doi.org/10.1021/acs.macromol.4c01402
Macromolecules 2024, 57, 8748−8762

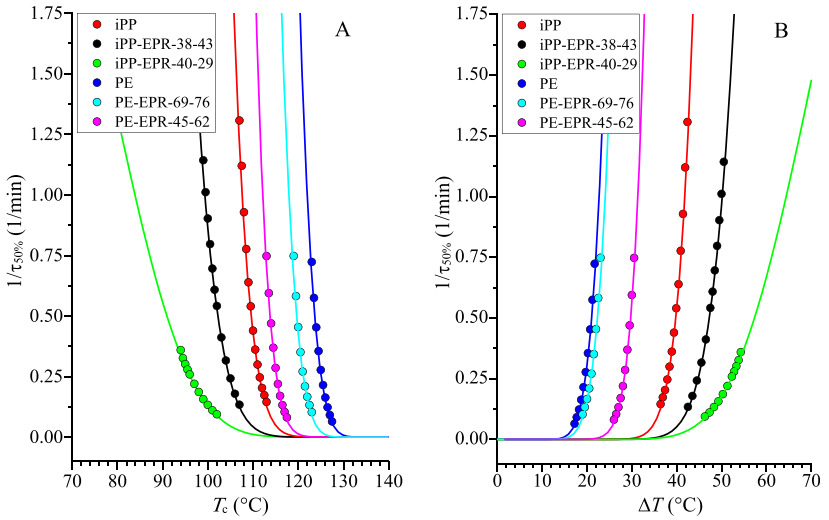

Figure 6. Overall crystallization rate as the inverse of the half crystallization time ($1/\tau_{50\%}$) as a function of the isothermal crystallization temperature T_c (A) and of the supercooling $\Delta T = T_m^0 - T_c$ (B) for samples of iPP and PE homopolymers and for iPP-*b*-EPR and PE-*b*-EPR BCPs. The lines are fits to the Lauritzen and Hoffman theory.

of the main melting peak corresponding to the melting of crystals of the iPP block.

Therefore, it is expected that the PE block crystallizes first also in the isothermal crystallization of Figures S14, S15, and S16, but crystallization until saturation of both blocks at the isothermal crystallization temperatures cannot be taken for granted. As in the nonisothermal crystallization of Figure 2, the presence in the DSC heating curves after isothermal crystallization of the sample iPP-PE-64 of Figure S16B of a main endothermic peak and a shoulder at higher temperature that can be attributed to melting of PE and iPP blocks, respectively, which have crystallized in the isothermal step, indicates that the iPP block of sample iPP-PE-64 can isothermally crystallize (or at least in part) during the isothermal steps. On the other hand, the heating curves of samples iPP-PE-52 and iPP-PE-60 (Figures S14B and S15B) display a single melting peak that could be related to the melting of only PE block or to the overlapped melting of both blocks.

To understand whether the iPP block crystallizes completely or in part in the employed ranges of T_c, the samples of iPP-*b*-PE block copolymers were kept at selected temperatures for the same crystallization times employed in the isothermal crystallization experiments reported in Figures S14–S16 and then successively cooled down to room temperature to reveal the crystallization of an eventual fraction of the BCP that was still in the melt (Figure 7).

All of the cooling scans of Figure 7 show exothermic peaks at nearly 102 °C, indicating that part of the iPP-*b*-PE copolymers do not crystallize during the isothermal step at the employed too high T_c but complete the crystallization during successive cooling. Since the crystallization temperature of 102 °C observed in the DSC cooling scans of Figure 7 is close to the T_c of the iPP homopolymer (curve c of Figure 2A), the exothermic peaks in Figure 7 may be related to the crystallization of the iPP block, or part of it, that does not crystallize at the isothermal crystallization temperature. This fraction of the sample that does not crystallize in the isothermal step and crystallizes afterward upon cooling increases with increasing T_c, as demonstrated by the increase of the crystallization enthalpy during cooling of Figure 7 with

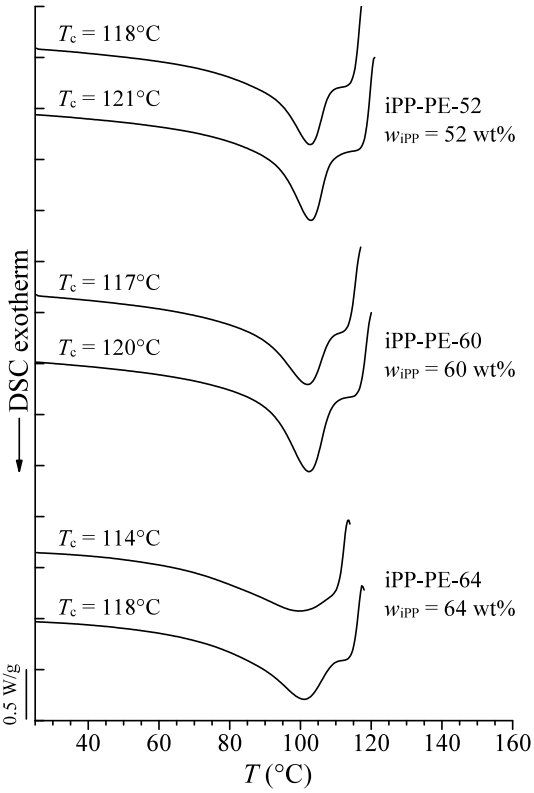

Figure 7. DSC cooling curves recorded at 20 °C/min after isothermal crystallization at selected T_c (for the same crystallization times employed in the isothermal crystallization experiments reported in Figures S14–S16) for samples iPP-PE-52, iPP-PE-60, and iPP-PE-64.

increasing T_c. For the sample iPP-PE-64 with a longer iPP block (w_{iPP} = 64 wt %), the enthalpy of the exothermic peaks in Figure 7 is lower compared to the other samples. This indicates that a lower amount of the sample crystallizes upon cooling, and a higher amount of the iPP block can crystallize in the isothermal step. Therefore, in iPP-*b*-PE BCPs, a fraction of the iPP component does not crystallize in the isothermal step,

https://doi.org/10.1021/acs.macromol.4c01402
Macromolecules 2024, 57, 8748−8762

and this fraction decreases with increasing weight fraction of the iPP block in the BCP.

The melting temperatures of the samples of iPP-*b*-PE BCPs isothermally crystallized from the melt, evaluated as described above and in SI, are reported in Figure 8 as a function of the

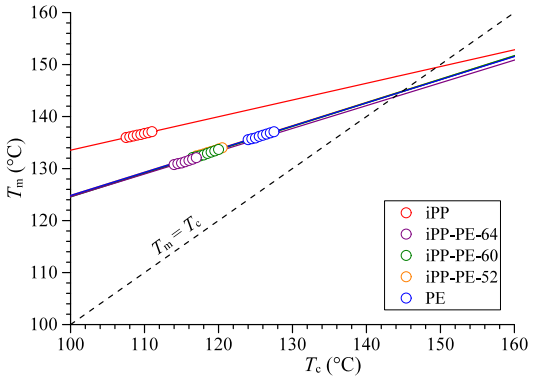

Figure 8. Hoffmann–Weeks linear fit of melting temperatures (T_m) as a function of the crystallization temperature (T_c) for the iPP and PE homopolymers and for the samples of iPP-*b*-PE BCPs.

crystallization temperature. The Hoffman–Weeks extrapolations of the melting temperature to the equilibrium melting temperatures are also shown. The obtained values of the equilibrium melting temperatures (T_m^0) of the BCPs, reported in Table S3, are comparable to the T_m^0 of the PE homopolymer, in agreement with the fact that during the isothermal crystallization of iPP-*b*-PE BCPs, the PE block is the main component that crystallizes.

The values of the inverse of the induction time $1/t_0$ (the nucleation rate) as a function of T_c and of the inverse of the half crystallization time $1/\tau_{50\%}$ (the crystallization rate) as a function of T_c and of the supercooling $\Delta T = T_m^0 - T_c$ for the samples of iPP-*b*-PE BCPs, evaluated from the crystallization exotherms of Figures S14A–S16A, are reported in Figures 9 and 10, respectively, in comparison with the data of the PE and iPP homopolymers. The equilibrium melting temperatures T_m^0 for the calculation of the supercooling are those of Table S3 and evaluated from the extrapolation of Figure 8. It is evident that the nucleation rates (Figure 9) and the overall

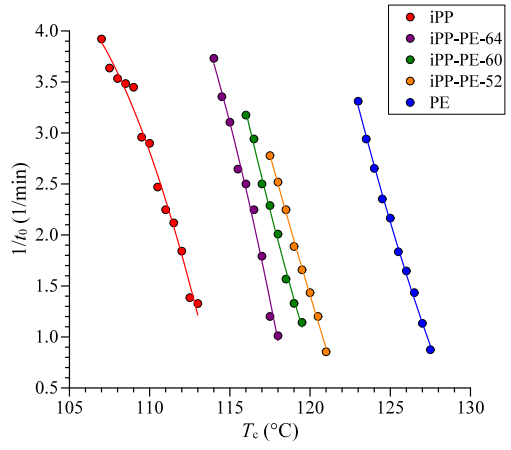

Figure 9. Inverse of the induction time ($1/t_0$) as a function of the isothermal crystallization temperature T_c for the iPP and PE homopolymers and iPP-*b*-PE BCPs.

crystallization rates (Figure 10) of the iPP-*b*-PE BCPs are intermediate between those of iPP and PE homopolymers.

The overall crystallization rate of the PE block in the BCPs is lower than that of the PE homopolymer due to the presence of the partially molten iPP block, and the crystallization rate at a given crystallization temperature decreases with increasing iPP weight fraction (Figure 11). At the same time, the fraction of the iPP block capable of crystallizing at the selected crystallization temperature T_c crystallizes faster with respect to the iPP homopolymer owing to the nucleation effect of the PE block, which crystallizes first and produces a nucleating effect on the iPP block crystals that accelerates the overall crystallization of the iPP block (see Figures 9 and 10).

Therefore, the overall crystallization kinetics of the PE block is slowed with respect to the PE homopolymer when it is linked to both amorphous EPR and semicrystalline iPP blocks. To compare the effect exerted on the PE block by the EPR and iPP attached blocks, the overall crystallization rates of PE-*b*-EPR and iPP-*b*-PE block copolymers are reported in Figure S22 as a function of T_c and of the supercooling. If we compare samples with similar weight fractions of PE, as samples PE-EPR-45-38 (w_{PE} = 45 wt %) and iPP-PE-60 (w_{PE} = 40 wt %), we conclude that the amorphous EPR block produces a greater slowdown of the overall crystallization kinetics of the PE block, compared to the semicrystalline iPP block.

The decrease of the overall crystallization rate observed in the double-crystalline iPP-*b*-PE copolymers with respect to PE homopolymer could suggest the existence of partial solubility between the blocks in the melt, although microphase-separated microstructures have been observed by TEM in iPP-*b*-PE BCPs,[17] and clear immiscibility between PE and iPP has been demonstrated in iPP/HDPE blends with interaction parameters in the melt in the range 0.03–0.10.[90−100] To clarify this point and verify the relative influences of the two iPP and PE components when they are not linked, a blend of iPP and PE homopolymers with a 50:50 composition has been prepared and isothermally crystallized at different temperatures. The blend was prepared as described in the SI employing the same two samples of iPP and PE homopolymers.

The DSC curves recorded during heating of the as-prepared sample of the blend, successive cooling from the melt, and subsequent heating are reported in Figure S23 of the SI. The melting behavior of the blend resembles that of the BCP sample iPP–PE-64, characterized by a main endothermic peak and a shoulder at higher temperature, which was attributed to the melting of iPP crystals. Contrary to the block copolymers, in the cooling scan of the blend, two exothermic peaks can be observed, where that one at higher temperatures of 118 °C can be surely attributed to the crystallization of PE, as the T_c is the same as that of the PE homopolymer, whereas the peak at a low temperature of 108.5 °C corresponds to the crystallization of the iPP. Therefore, the iPP component of the blend crystallizes at temperature (108.5 °C) higher than that of the iPP homopolymer (102 °C, see Table 2 and curve c of Figure 2A). This effect is clearly attributable to the nucleation effect of PE crystallized before on the subsequent crystallization of iPP.

This sample of the blend was isothermally crystallized at selected crystallization temperatures. The DSC crystallization exotherms recorded during the isothermal crystallizations at different T_c and the subsequent DSC heating curves of the crystallized samples are reported in Figure S24 of the SI. A single melting peak is observed for all crystallization temperatures in the heating curves in Figure S24B. The absence of the

https://doi.org/10.1021/acs.macromol.4c01402
Macromolecules 2024, 57, 8748−8762

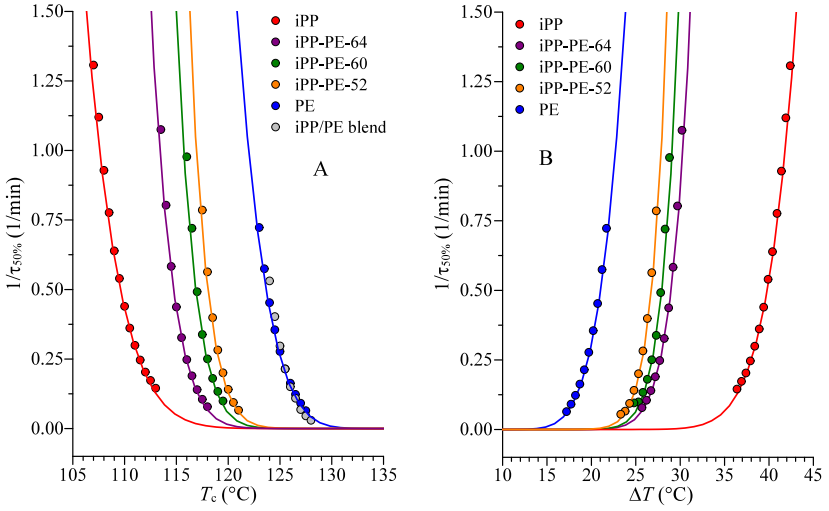

Figure 10. Overall crystallization rate as inverse of the half crystallization time $(1/\tau_{50\%})$ as a function of the isothermal crystallization temperature T_c (A) and of the supercooling $\Delta T = T_m^0 - T_c$ (B) for samples of iPP and PE homopolymers, iPP-*b*-PE BCPs and of the 50:50 iPP/PE blend. The solid lines represent fits to the Lauritzen and Hoffman theory.

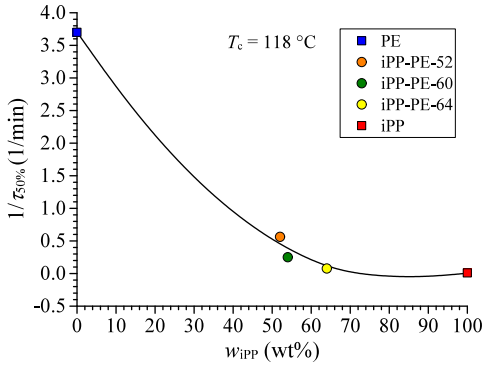

Figure 11. Inverse of half crystallization time $(1/\tau_{50\%})$ as a function of iPP weight fraction for iPP-*b*-PE BCPs and iPP and PE homopolymers at a constant crystallization temperature of 118 °C. The circles represent experimental values, whereas the squares represent the values predicted by the Lauritzen and Hoffman fitting.

shoulder at higher temperatures suggests that the iPP block does not crystallize in the isothermal steps. This is confirmed by parallel experiments, where the blend sample was cooled down to 25 °C after the isothermal crystallization at 125 and 127 °C (Figure S25). Both the cooling curves show an exothermic peak that can be attributed to the crystallization of iPP that has not crystallized in the isothermal step. The crystallization enthalpy does not change with the crystallization temperature, indicating that all of the iPP component in the blend does not crystallize in the isothermal step, not even at the lower T_c, and crystallizes completely during successive cooling. Moreover, a minor exothermic peak can be observed at higher temperatures in the cooling curves of Figure S25 that could be related to the crystallization of a fraction of the PE.

The curves of the overall crystallization kinetics of the blend are shown in Figure S26, and the values of the overall crystallization rate $(1/\tau_{50\%})$ are plotted as a function of T_c together with the data of iPP-*b*-PE block copolymers and PE and iPP homopolymers in Figure 10A. It is immediately apparent that when the two homopolymers are blended, the kinetics of crystallization of PE in the presence of iPP is identical with that of the neat PE homopolymer. This result indicates that, in the blend, the presence of iPP does not affect the crystallization rate of PE, confirming the phase-separation in the melt due to immiscibility between PE and iPP.[90−100] Therefore, the slowdown of the overall crystallization kinetics of PE in the iPP-*b*-PE BCPs due to the influence of iPP can be ascribed uniquely to the constraint generated by the covalently bonded iPP block and not to the partial miscibility between the blocks.

CONCLUSIONS

Samples of crystalline−crystalline BCPs made of iPP and PE blocks (iPP-*b*-PE) and of crystalline−amorphous BCPs comprising semicrystalline blocks of iPP or PE linked to an amorphous block of EPR (iPP-*b*-EPR and PE-*b*-EPR) of different lengths of the blocks and ethylene concentrations in EPR blocks have been synthesized with different catalysts. The crystallization behaviors of the BCP samples and the influence of the molecular structure and topology of the BCPs on the crystallization kinetics of iPP and PE have been analyzed.

Due to its moderate stereoregularity, the iPP block melts at a low temperature of 135 °C, similar to that of the PE block. Although the iPP and PE blocks crystallize and melt within a similar temperature range, the PE block crystallizes first and drives the crystallization of the iPP block through a nucleation effect.

The iPP-*b*-EPR and PE-*b*-EPR copolymers show lower crystallization temperatures with respect to those of the iPP and PE homopolymers, respectively, due to partial miscibility between the crystallizable block and the amorphous EPR phase. Moreover, the decrease of the ethylene concentration in the EPR block of iPP-*b*-EPR copolymers results in a further decrease of crystallization temperature due to the increased solubility in the melt between iPP and EPR blocks with decreasing ethylene concentration in the EPR.

All samples have been crystallized at different isothermal crystallization temperatures, and the crystallization kinetics have been analyzed, allowing one to understand how the different blocks mutually influence their crystallization rates. The kinetics data were processed using the Avrami and Lauritzen−Hoffman models. The equilibrium melting temperatures of iPP and PE blocks in the BCPs, evaluated with the

https://doi.org/10.1021/acs.macromol.4c01402
Macromolecules 2024, 57, 8748−8762

Hoffman−Weeks extrapolation, are very close to those of the homopolymers.

In both the iPP-*b*-EPR and PE-*b*-EPR BCPs, the presence of a covalently linked amorphous EPR block drastically slows the overall crystallization rate of the iPP and PE blocks, with respect to the corresponding iPP and PE homopolymers. Furthermore, in iPP-*b*-EPR samples, a higher concentration of propylene in the EPR phase results in a greater slowdown of the crystallization kinetics of iPP due to a higher solubility between the blocks. Analogously, in PE-*b*-EPR copolymers, the increase in the length of the EPR block results in a greater slowdown of the crystallization rate of the PE with respect to the PE homopolymer due to major dilution exerted by the long EPR block.

Finally, the crystallization rates of iPP-*b*-PE copolymers are lower than that of the PE homopolymer but faster than that of the iPP homopolymer. In the isothermal crystallizations, the iPP blocks do not crystallize, not even at low crystallization temperatures, but crystallize upon successive cooling, nucleating over the PE crystals formed in the isothermal step. Therefore, the linked iPP block, which remains in the melt or crystallizes partially during the isothermal crystallization, slows down the crystallization kinetics of PE, in contrast to what happens in the iPP/PE blend, where the crystallization kinetics of PE is not affected by the presence of the phase-separated iPP. This indicates that the slowdown of the overall crystallization kinetics of PE in the iPP-*b*-PE BCPs can be ascribed uniquely to the constraint generated by the covalently linked iPP block and not to the partial miscibility between the blocks.

■ ASSOCIATED CONTENT

Supporting Information

The Supporting Information is available free of charge at https://pubs.acs.org/doi/10.1021/acs.macromol.4c01402.

Experimental details about the synthesis of iPP-*b*-EPR, PE-*b*-EPR, and iPP-*b*-PE block copolymer samples and of the characterization by gel permeation chromatography (GPC) and ^{13}C NMR; Details of experiments of wide-angle X-ray diffraction, polarized light optical microscopy (PLOM), differential scanning calorimetry (DSC), isothermal crystallization from the melt and of the procedure for the analysis of the crystallization kinetics; Experimental method for the preparation of the 50/50 iPP/PE blend; ^{13}C NMR spectra of the iPP homopolymer and of the samples of iPP-*b*-EPR, PE-*b*-EPR, and iPP-*b*-PE block copolymers; Analysis of the ^{13}C NMR spectra and assignment of all signals to evaluate the composition of the BCPs, lengths of blocks and concentration of ethylene in the EPR blocks; Additional DSC data; Additional PLOM images; Complete DSC data of isothermal crystallizations and analysis of the crystallization kinetics (PDF)

■ AUTHOR INFORMATION

Corresponding Authors

Rocco Di Girolamo − *Dipartimento di Scienze Chimiche, Università di Napoli Federico II, I-80126 Napoli, Italy;* orcid.org/0000-0001-8815-2997; Email: rocco.digirolamo@unina.it

Claudio De Rosa − *Dipartimento di Scienze Chimiche, Università di Napoli Federico II, I-80126 Napoli, Italy;* orcid.org/0000-0002-5375-7475; Email: claudio.derosa@unina.it

Authors

Alessandra Cicolella − *Dipartimento di Scienze Chimiche, Università di Napoli Federico II, I-80126 Napoli, Italy; Scuola Superiore Meridionale, I-80138 Napoli, Italy;* orcid.org/0000-0002-1821-8134

Miriam Scoti − *Dipartimento di Scienze Chimiche, Università di Napoli Federico II, I-80126 Napoli, Italy;* orcid.org/0000-0001-9225-1509

Giovanni Talarico − *Dipartimento di Scienze Chimiche, Università di Napoli Federico II, I-80126 Napoli, Italy;* orcid.org/0000-0002-4861-0444

Alejandro J. Müller − *POLYMAT and Department of Polymers and Advanced Materials: Physics, Chemistry and Technology, Faculty of Chemistry, University of the Basque Country UPV/EHU, 20018 Donostia-San Sebastián, Spain; IKERBASQUE, Basque Foundation for Science, 48009 Bilbao, Spain;* orcid.org/0000-0001-7009-7715

Complete contact information is available at: https://pubs.acs.org/10.1021/acs.macromol.4c01402

Notes

The authors declare no competing financial interest.

■ ACKNOWLEDGMENTS

The task force "Polymers and biopolymers" of the University of Napoli Federico II is acknowledged. A.J.M. acknowledges funding from the Basque Government through Grant IT1503-22. We thank Prof. Geoffrey W. Coates of Cornell University, Ithaca, New York, for providing the BCP samples.

■ REFERENCES

(1) Hamley, I. W. *The Physics of Block Copolymers*; Oxford University Press, 1998.

(2) Hamley, I. W. Introduction to Block Copolymers. In *Developments in Block Copolymer Science and Technology*; Hamley, I. W., Ed.; John Wiley & Sons: Chichester, 2004; pp 1−29.

(3) De Rosa, C.; Park, C.; Thomas, E. L.; Lotz, B. Microdomain patterns via directional eutectic solidification and epitaxy. *Nature* **2000**, *405*, 433.

(4) Loo, Y.-L.; Register, R. A. Crystallization within Block Copolymer Mesophases. In *Developments in Block Copolymer Science and Technology*; Hamley, I. W., Ed.; John Wiley & Sons: Chichester, 2004; pp 213−243.

(5) Loo, Y.-L.; Register, R. A.; Ryan, A. J. Modes of Crystallization in Block Copolymer Microdomains: Breakout, Templated, and Confined. *Macromolecules* **2002**, *35*, 2365−2374.

(6) Müller, A. J.; Balsamo, V.; Arnal, M. L. Nucleation and Crystallization in Diblock and Triblock Copolymers. *Adv. Polym. Sci.* **2005**, *190*, 1−63.

(7) Müller, A. J.; Arnal, M. L.; Balsamo, V. Crystallization in Block Copolymers with More than One Crystallizable Block. In *Progress in Understanding of Polymer Crystallization, Lecture Notes in Physics*; Reiter, G., Strobl, G. R., Eds.; Springer-Verlag: Berlin, 2007; pp 229−259.

(8) Castillo, R. V.; Müller, A. J. Crystallization and Morphology of Biodegradable or Biostable Single and Double Crystalline Block Copolymers. *Prog. Polym. Sci.* **2009**, *34*, 516−560.

(9) Palacios, J. K.; Mugica, A.; Zubitur, M.; Müller, A. J. Crystallization and Morphology of Block Copolymers and Terpolymers with More than One Crystallizable Block. *Crystallization in Multiphase Polymer Systems*; Elsevier Inc., 2018; pp 123−180.

(10) Li, S.; Register, R. A. Crystallization in Copolymers. In *Handbook of Polymer Crystallization*; Piorkowska, E., Rutledge, G. C., Eds.; John Wiley & Sons, Inc.: Hoboken, NJ, 2013; pp 327−346.
(11) De Rosa, C.; Di Girolamo, R.; Malafronte, A.; Scoti, M.; Talarico, G.; Auriemma, F.; Ruiz de Ballesteros, O. Polyolefins Based Crystalline Block Copolymers: Ordered Nanostructures from Control of Crystallization. *Polymer* **2020**, *196*, 122423.
(12) De Rosa, C.; Auriemma, F.; Di Girolamo, R.; Aprea, R.; Thierry, A. Selective Gold Deposition on a Nanostructured Block Copolymer Film Crystallized by Epitaxy. *Nano Res.* **2011**, *4*, 241−248.
(13) De Rosa, C.; Di Girolamo, R.; Auriemma, F.; D'Avino, M.; Talarico, G.; Cioce, C.; Scoti, M.; Coates, G. W.; Lotz, B. Oriented Microstructures of Crystalline−Crystalline Block Copolymers Induced by Epitaxy and Competitive and Confined Crystallization. *Macromolecules* **2016**, *49*, 5576−5586.
(14) De Rosa, C.; Di Girolamo, R.; Auriemma, F.; Talarico, G.; Malafronte, A.; Scarica, C.; Scoti, M. Controlling Size and Orientation of Lamellar Microdomains in Crystalline Block Copolymers. *ACS Appl. Mater. Interfaces* **2017**, *9*, 31252−31259.
(15) De Rosa, C.; Di Girolamo, R.; Cicolella, A.; Talarico, G.; Scoti, M. Double Crystallization and Phase Separation in Polyethylene—Syndiotactic Polypropylene Di-Block Copolymers. *Polymers* **2021**, *13*, 2589.
(16) Di Girolamo, R.; Cicolella, A.; Talarico, G.; Scoti, M.; De Stefano, F.; Giordano, A.; Malafronte, A.; De Rosa, C. Structure and Morphology of Crystalline Syndiotactic Polypropylene-Polyethylene Block Copolymers. *Polymers* **2022**, *14*, 1534.
(17) De Rosa, C.; Malafronte, A.; Di Girolamo, R.; Auriemma, F.; Scoti, M.; Ruiz de Ballesteros, O.; Coates, G. W. Morphology of Isotactic Polypropylene−Polyethylene Block Copolymers Driven by Controlled Crystallization. *Macromolecules* **2020**, *53*, 10234−10244.
(18) Di Girolamo, R.; Santillo, C.; Malafronte, A.; Scoti, M.; De Stefano, F.; Talarico, G.; Coates, G. W.; De Rosa, C. Structure and Morphology of Isotactic Polypropylene−Polyethylene Block Copolymers Prepared with Living and Stereoselective Catalyst. *Polym. Chem.* **2022**, *13*, 2950−2963.
(19) Cicolella, A.; De Stefano, F.; Scoti, M.; Talarico, G.; Eagan, J. M.; Coates, G. W.; Di Girolamo, R.; De Rosa, C. Phase Separation and Crystallization in Monodisperse Block Copolymers of Linear Low-Density Polyethylene and Isotactic Polypropylene. *Macromolecules* **2024**, *57*, 2230−2245.
(20) Bates, F. S.; Fredrickson, G. H. Block Copolymer Thermodynamics: Theory and Experiment. *Annu. Rev. Phys. Chem.* **1990**, *41*, 525−557.
(21) Bates, F. S. Polymer-Polymer Phase Behavior. *Science* **1991**, *251*, 898−905.
(22) Hamley, I. W. Crystallization in Block Copolymers. *In Interfaces Crystallization Viscoelasticity Adv. Polym. Sci.* **1999**, *148*, 113−137.
(23) Nojima, S.; Nakano, H.; Ashida, T. Crystallization Behavior of a Microphase-Separated Diblock Copolymer. *Polymer* **1993**, *34*, 4168−4170.
(24) Quiram, D. J.; Register, R. A.; Marchand, G. R.; Adamson, D. H. Chain Orientation in Block Copolymers Exhibiting Cylindrically Confined Crystallization. *Macromolecules* **1998**, *31*, 4891−4898.
(25) Rangarajan, P.; Register, R. A.; Fetters, L. J.; Bras, W.; Naylor, S.; Ryan, A. J. Crystallization of a Weakly Segregated Polyolefin Diblock Copolymer. *Macromolecules* **1995**, *28*, 4932−4938.
(26) Nojima, S.; Kato, K.; Yamamoto, S.; Ashida, T. Crystallization of Block Copolymers. 1.Small-Angle X-Ray Scattering Study of a. Epsilon-Caprolactone-Butadiene Diblock Copolymer. *Macromolecules* **1992**, *25*, 2237−2242.
(27) Castillo, R. V.; Muller, A. J.; Raquez, J.-M.; Dubois, P. Crystallization Kinetics and Morphology of Biodegradable Double Crystalline PLLA-b-PCL Diblock Copolymers. *Macromolecules* **2010**, *43*, 4149−4160.
(28) Müller, A. J.; Lorenzo, A. T.; Castillo, R. V.; Arnal, M. L.; Boschetti-de-Fierro, A.; Abetz, V. Crystallization Kinetics of Homogeneous and Melt Segregated PE Containing Diblock Copolymers. *Macromol. Symp.* **2006**, *245*, 154−160.
(29) Müller, A. J.; Albuerne, J.; Esteves, L. M.; Marquez, L.; Raquez, J.; Degée, P.; Dubois, P.; Collins, S.; Hamley, I. W. Confinement Effects on the Crystallization Kinetics and Self-Nucleation of Double Crystalline Poly (P-dioxanone)-b-poly (ε-caprolactone) Diblock Copolymers. *Macromol. Symp.* **2004**, *215*, 369−382.
(30) Sun, L.; Liu, Y.; Zhu, L.; Hsiao, B. S.; Avila-Orta, C. A. Self-Assembly and Crystallization Behavior of a Double-Crystalline Polyethylene-Block-Poly (Ethylene Oxide) Diblock Copolymer. *Polymer* **2004**, *45*, 8181−8193.
(31) Castillo, R. V.; Muller, A. J.; Lin, M.-C.; Chen, H.-L.; Jeng, U.-S.; Hillmyer, M. A. Confined Crystallization and Morphology of Melt Segregated PLLA-b-PE and PLDA-b-PE Diblock Copolymers. *Macromolecules* **2008**, *41*, 6154−6164.
(32) Bao, J.; Dong, X.; Chen, S.; Lu, W.; Zhang, X.; Chen, W. Confined Crystallization, Melting Behavior and Morphology in PEG-b-PLA Diblock Copolymers: Amorphous versus Crystalline PLA. *J. Polym. Sci.* **2020**, *58*, 455−465.
(33) Myers, S. B.; Register, R. A. Crystalline−Crystalline Diblock Copolymers of Linear Polyethylene and Hydrogenated Polynorbornene. *Macromolecules* **2008**, *41*, 6773−6779.
(34) Li, S.; Register, R. A.; Landes, B. G.; Hustad, P. D.; Weinhold, J. D. Crystallization in Ordered Polydisperse Polyolefin Diblock Copolymers. *Macromolecules* **2010**, *43*, 4761−4770.
(35) Park, H. E.; Dealy, J. M.; Marchand, G. R.; Wang, J.; Li, S.; Register, R. A. Rheology and Structure of Molten, Olefin Multiblock Copolymers. *Macromolecules* **2010**, *43*, 6789−6799.
(36) Li, S.; Register, R. A.; Weinhold, J. D.; Landes, B. G. Melt and Solid-State Structures of Polydisperse Polyolefin Multiblock Copolymers. *Macromolecules* **2012**, *45*, 5773−5781.
(37) Wen, T.; Liu, G.; Zhou, Y.; Zhang, X.; Wang, F.; Chen, H.; Loos, J.; Wang, D. Epitaxy-Induced Crystallization of Olefin Block Copolymers. *Macromolecules* **2012**, *45*, 5979−5985.
(38) Wen, T.; Zhou, Y.; Liu, G.; Wang, F.; Zhang, X.; Wang, D.; Chen, H.; Walton, K.; Marchand, G.; Loos, J. Epitaxial Crystallization of Olefin Block Copolymers (OBCs) on Uniaxially Oriented Isotactic Polypropylene and High-Density Polyethylene Films. *Polymer* **2012**, *53*, 529−535.
(39) Auriemma, F.; De Rosa, C.; Scoti, M.; Di Girolamo, R.; Malafronte, A.; Talarico, G.; Carnahan, E. Unveiling the Molecular Structure of Ethylene/1-Octene Multi-Block Copolymers from Chain Shuttling Technology. *Polymer* **2018**, *154*, 298−304.
(40) Auriemma, F.; De Rosa, C.; Scoti, M.; Di Girolamo, R.; Malafronte, A.; Galotto Galotto, N. Structural Investigation at Nanometric Length Scale of Ethylene/1-Octene Multiblock Copolymers from Chain-Shuttling Technology. *Macromolecules* **2018**, *51*, 9613−9625.
(41) Auriemma, F.; De Rosa, C.; Scoti, M.; Di Girolamo, R.; Malafronte, A.; D'Alterio, M. C.; Boggioni, L.; Losio, S.; Boccia, A. C.; Tritto, I. Structure and Mechanical Properties of Ethylene/1-Octene Multiblock Copolymers from Chain Shuttling Technology. *Macromolecules* **2019**, *52*, 2669−2680.
(42) Auriemma, F.; Di Girolamo, R.; Urciuoli, G.; Caputo, M. R.; De Rosa, C.; Scoti, M.; Malafronte, A.; Cipullo, R.; Busico, V.; Grizzuti, N.; et al. Transmission Electron Microscopy Analysis of Multiblock Ethylene/1-Octene Copolymers. *Polymer* **2020**, *193*, 122347.
(43) Cho, K.; Li, F.; Choi, J. Crystallization and Melting Behavior of Polypropylene and Maleated Polypropylene Blends. *Polymer* **1999**, *40*, 1719−1729.
(44) Furushima, Y.; Nakada, M.; Masuda, A.; Okada, K.; Iwata, N.; Ohkura, M. Isothermal Crystallization Kinetics, Morphology, and Crystalline Structure of Polypropylene/Poly(4-methyl-1-pentene) Blends. *Polymer Crystallization* **2020**, *3*, No. e10102.
(45) Campoy, I.; Arribas, J. M.; Zaporta, M. A. M.; Marco, C.; Gomez, M. A.; Fatou, J. G. Crystallization Kinetics of Polypropylene-Polyamide Compatibilized Blends. *Eur. Polym. J.* **1995**, *31*, 475−480.
(46) Luo, D.-J.; Shao, H.-J.; Wei, F.-J.; Zhang, K.-Z.; Cui, Z.-Y.; Yu, J.; Qin, S.-H. Morphology and Isothermal Crystallization Kinetics of

https://doi.org/10.1021/acs.macromol.4c01402
Macromolecules 2024, 57, 8748−8762

Polypropylene/Poly (Ethylene-Co-Vinyl Alcohol) Blends. *Int. Polym. Process.* **2019**, *34*, 195−208.
(47) Cai, J.; Luo, R.; Lv, R.; He, Y.; Zhou, D.; Hu, W. Crystallization Kinetics of Ethylene-Co-Propylene Rubber/Isotactic Polypropylene Blend Investigated via Chip-Calorimeter Measurement. *Eur. Polym. J.* **2017**, *96*, 79−86.
(48) Svoboda, P.; Svobodova, D.; Slobodian, P.; Ougizawa, T.; Inoue, T. Crystallization Kinetics of Polypropylene/Ethylene−Octene Copolymer Blends. *Polym. Test* **2009**, *28*, 215−222.
(49) Avalos, F.; Lopez-Manchado, M. A.; Arroyo, M. Crystallization Kinetics of Polypropylene: 1. Effect of Small Additions of Low-Density Polyethylene. *Polymer* **1996**, *37*, 5681−5688.
(50) Huang, D. E.; Kotula, A. P.; Snyder, C. R.; Migler, K. B. Crystallization Kinetics in an Immiscible Polyolefin Blend. *Macromolecules* **2022**, *55*, 10921−10932.
(51) Coba-Daza, S.; Carmeli, E.; Otaegi, I.; Aranburu, N.; Guerrica-Echevarria, G.; Kahlen, S.; Cavallo, D.; Tranchida, D.; Müller, A. J. Effect of Compatibilizer Addition on the Surface Nucleation of Dispersed Polyethylene Droplets in a Self-Nucleated Polypropylene Matrix. *Polymer* **2022**, *263*, 125511.
(52) Fenni, S. E.; Müller, A. J.; Cavallo, D. Understanding Polymer Nucleation by Studying Droplets Crystallization in Immiscible Polymer Blends. *Polymer* **2023**, *264*, 125514.
(53) Tian, J.; Hustad, P. D.; Coates, G. W. A New Catalyst for Highly Syndiospecific Living Olefin Polymerization: Homopolymers and Block Copolymers from Ethylene and Propylene. *J. Am. Chem. Soc.* **2001**, *123*, 5134−5135.
(54) Coates, G. W.; Hustad, P. D.; Reinartz, S. Catalysts for the Living Insertion Polymerization of Alkenes: Access to New Polyolefin Architectures Using Ziegler−Natta Chemistry. *Ang. Chem. Int. Ed.* **2002**, *41*, 2236−2257.
(55) Domski, G. J.; Lobkovsky, E. B.; Coates, G. W. Polymerization of α-Olefins with Pyridylamidohafnium Catalysts: Living Behavior and Unexpected Isoselectivity from a C s-Symmetric Catalyst Precursor. *Macromolecules* **2007**, *40*, 3510−3513.
(56) Domski, G. J.; Rose, J. M.; Coates, G. W.; Bolig, A. D.; Brookhart, M. Living Alkene Polymerization: New Methods for the Precision Synthesis of Polyolefins. *Prog. Polym. Sci.* **2007**, *32*, 30−92.
(57) De Rosa, C.; Di Girolamo, R.; Talarico, G. Expanding the Origin of Stereocontrol in Propene Polymerization Catalysis. *ACS Catal.* **2016**, *6*, 3767−3770.
(58) Domski, G. J.; Eagan, J. M.; De Rosa, C.; Di Girolamo, R.; LaPointe, A. M.; Lobkovsky, E. B.; Talarico, G.; Coates, G. W. Combined Experimental and Theoretical Approach for Living and Isoselective Propylene Polymerization. *ACS Catal.* **2017**, *7*, 6930−6937.
(59) Eagan, J. M.; Xu, J.; Di Girolamo, R.; Thurber, C. M.; Macosko, C. W.; LaPointe, A. M.; Bates, F. S.; Coates, G. W. Combining Polyethylene and Polypropylene: Enhanced Performance with PE/i PP Multiblock Polymers. *Science* **2017**, *355*, 814−816.
(60) Xu, J.; Eagan, J. M.; Kim, S.-S.; Pan, S.; Lee, B.; Klimovica, K.; Jin, K.; Lin, T.-W.; Howard, M. J.; Ellison, C. J.; et al. Compatibilization of Isotactic Polypropylene (iPP) and High-Density Polyethylene (HDPE) with iPP−PE Multiblock Copolymers. *Macromolecules* **2018**, *51*, 8585−8596.
(61) Matsui, S.; Tohi, Y.; Mitani, M.; Saito, J.; Makio, H.; Tanaka, H.; Nitabaru, M.; Nakano, T.; Fujita, T. New Bis (Salicylaldiminato) Titanium Complexes for Ethylene Polymerization. *Chem. Lett.* **1999**, *28*, 1065−1066.
(62) Mitani, M.; Mohri, J.; Yoshida, Y.; Saito, J.; Ishii, S.; Tsuru, K.; Matsui, S.; Furuyama, R.; Nakano, T.; Tanaka, H.; et al. Living Polymerization of Ethylene Catalyzed by Titanium Complexes Having Fluorine-Containing Phenoxy−Imine Chelate Ligands. *J. Am. Chem. Soc.* **2002**, *124*, 3327−3336.
(63) De Rosa, C.; Scoti, M.; Di Girolamo, R.; Ballesteros, O. R.; Auriemma, F.; Malafronte, A. Polymorphism in Polymers: A Tool to Tailor Material's Properties. *Polymer Crystallization* **2020**, *3*, No. e10101.
(64) Auriemma, F.; De Rosa, C.; Malafronte, A.; Scoti, M.; Di Girolamo, R. Solid State Polymorphism of Isotactic and Syndiotactic Polypropylene. In *Polypropylene Handbook: Morphology, Blends and Composites*; Karger-Kocsis, J., Bárány, T., Eds.; Springer, 2019; pp 37−119.
(65) Bunn, C. W. The Crystal Structure of Long-Chain Normal Paraffin Hydrocarbons. The "Shape" of the CH2 Group. *Trans. Faraday Soc.* **1939**, *35*, 482−491.
(66) Hua, X.; Cheng, J.; Wang, Y.; Liu, L.-Z.; Wang, Y.; Shi, Y. Crystallization, Structure and Properties of PP-b-PE Block Copolymer. *Polymer* **2023**, *284*, 126310.
(67) Scoti, M.; De Stefano, F.; Di Girolamo, R.; Malafronte, A.; Talarico, G.; De Rosa, C. Model of Crystallization Behavior of Isotactic Polypropylene: The Role of Defects. *Macromol. Chem. Phys.* **2023**, *224*, 2200262.
(68) Scoti, M.; De Stefano, F.; Talarico, G.; De Rosa, C. The genetics in polymers: Crystallization as a fingerprint of the molecular microstructure. *Polymer* **2024**, *293*, 126637.
(69) Alamo, R. G.; Kim, M. H.; Galante, M. J.; Isasi, J. R.; Mandelkern, L. Structural and Kinetic Factors Governing the Formation of the γ Polymorph of Isotactic Polypropylene. *Macromolecules* **1999**, *32*, 4050−4064.
(70) De Rosa, C.; Auriemma, F.; Di Capua, A.; Resconi, L.; Guidotti, S.; Camurati, I.; Nifant'ev, I. E.; Laishevtsev, I. P. Structure-property correlations in polypropylene from metallocene catalysts: stereodefective, regioregular isotactic polypropylene. *J. Am. Chem. Soc.* **2004**, *126*, 17040−17049.
(71) De Rosa, C.; Auriemma, F. Structural-mechanical phase diagram of isotactic polypropylene. *J. Am. Chem. Soc.* **2006**, *128*, 11024.
(72) Cicolella, A.; De Stefano, F.; Scoti, M.; De Rosa, C. Self-Nucleation in Stereodefective Isotactic Polypropylene: The Impact of Stereodefects on the Melt Memory. *Macromolecules* **2024**, *57*, 1653−1666.
(73) Cicolella, A.; De Rosa, C.; Sepe, E.; De Stefano, F.; Giordano, A.; Scoti, M. The Impact of Regiodefects on the Melt Memory of Isotactic Polypropylene. *Macromol. Rapid Commun.* **2024**, *45*, 2400233.
(74) De Rosa, C.; Auriemma, F.; Ruiz de Ballesteros, O.; Resconi, L.; Camurati, I. Crystallization Behavior of Isotactic Propylene-Ethylene and Propylene-Butene Copolymers: Effect of Comonomers *versus* Stereodefects on Crystallization Properties of Isotactic Polypropylene. *Macromolecules* **2007**, *40*, 6600.
(75) De Rosa, C.; Auriemma, F.; Talarico, G.; Ruiz de Ballesteros, O. Structure of isotactic propylene-pentene copolymers. *Macromolecules* **2007**, *40*, 8531−8532.
(76) Auriemma, F.; De Rosa, C.; Di Girolamo, R.; Malafronte, A.; Scoti, M.; Cipullo, R. Yield behavior of random copolymers of isotactic polypropylene. *Polymer* **2017**, *129*, 235−246.
(77) Auriemma, F.; De Rosa, C.; Di Girolamo, R.; Malafronte, A.; Scoti, M.; Cioce, C. A molecular view of properties of random copolymers of isotactic polypropene. *Adv. Polym. Sci.* **2016**, *276*, 45−92.
(78) De Rosa, C.; Scoti, M.; Auriemma, F.; Ruiz de Ballesteros, O.; Talarico, G.; Malafronte, A.; Di Girolamo, R. Mechanical Properties and Morphology of Propene−Pentene Isotactic Copolymers. *Macromolecules* **2018**, *51*, 3030−3040.
(79) De Rosa, C.; Scoti, M.; Auriemma, F.; Ruiz de Ballesteros, O.; Talarico, G.; Di Girolamo, R.; Cipullo, R. Relationships among lamellar morphology parameters, structure and thermal behavior of isotactic propene-pentene copolymers: The role of incorporation of comonomeric units in the crystals. *Eur. Polym. J.* **2018**, *103*, 251−259.
(80) Scoti, M.; De Stefano, F.; Di Girolamo, R.; Talarico, G.; Malafronte, A.; De Rosa, C. Crystallization of Propene-Pentene Isotactic Copolymers as an Indicator of the General View of the Crystallization Behavior of Isotactic Polypropylene. *Macromolecules* **2022**, *55*, 241.

https://doi.org/10.1021/acs.macromol.4c01402
Macromolecules 2024, 57, 8748−8762

(81) Scoti, M.; De Stefano, F.; Giordano, A.; Talarico, G.; De Rosa, C. Crystallization Behavior of Isotactic Propene-Octene Random Copolymers. *Polymers* **2022**, *14*, 4032.
(82) Scoti, M.; De Stefano, F.; Di Girolamo, R.; Malafronte, A.; Talarico, G.; De Rosa, C. Crystallization Behavior and Properties of Propylene/4-Methyl-1-pentene Copolymers from a Metallocene Catalyst. *Macromolecules* **2023**, *56*, 1446−1460.
(83) De Rosa, C.; Auriemma, F.; Di Girolamo, R.; Ruiz de Ballesteros, O.; Pepe, M.; Tarallo, O.; Malafronte, A. Morphology and Mechanical Properties of the Mesomorphic Form of Isotactic Polypropylene in Stereodefective Polypropylene. *Macromolecules* **2013**, *46*, 5202−5214.
(84) Auriemma, F.; De Rosa, C.; Di Girolamo, R.; Malafronte, A.; Scoti, M.; Mitchell, G. R.; Esposito, S. Relationship between molecular configuration and stress induced phase transitions. In *Controlling the Morphology of Polymers - Multiple Scales of Structure and Processing*; Mitchell, G. R., Tojeira, A., Eds.; Springer International Publishing, 2016; p 287.
(85) Geil, P. H. *Polymer Single Crystals*; Interscience (Wiley): New York, 1963.
(86) Gedde, U. L. F. *Polymer Physics*; Springer Science & Business Media, 1995.
(87) Keith, H. D.; Padden, F. J., Jr A Phenomenological Theory of Spherulitic Crystallization. *J. Appl. Phys.* **1963**, *34* (8), 2409−2421.
(88) Keith, H. D.; Padden, F. J., Jr The Optical Behavior of Spherulites in Crystalline Polymers. Part I. Calculation of Theoretical Extinction Patterns in Spherulites with Twisting Crystalline Orientation. *J. Polym. Sci.* **1959**, *39*, 101−122.
(89) Crist, B.; Schultz, J. M. Polymer Spherulites: A Critical Review. *Prog. Polym. Sci.* **2016**, *56*, 1−63.
(90) Zhao, L.; Choi, P. Measurement of solvent-independent polymer−polymer Flory−Huggins interaction parameters with the use of non-random partitioning solvents in inverse gas chromatography. *Polymer* **2002**, *43*, 6677−6681.
(91) Jose, S.; Aprem, A. S.; Francis, B.; Chandy, M. C.; Werner, P.; Alstaedt, V.; Thomas, S. Phase Morphology, Crystallization Behavior and Mechanical Properties of Isotactic Polypropylene/High Density Polyethylene Blends. *Eur. Polym. J.* **2004**, *40*, 2105−2115.
(92) Choi, P.; Blom, H. P.; Kavassalis, T. A.; Rudin, A. Immiscibility of Poly (Ethylene) and Poly (Propylene): A Molecular Dynamics Study. *Macromolecules* **1995**, *28*, 8247−8250.
(93) Wignall, G. D.; Child, H. R.; Samuels, R. J. Structural Characterization of Semicrystalline Polymer Blends by Small-Angle Neutron Scattering. *Polymer* **1982**, *23*, 957−964.
(94) Jeon, H. S.; Lee, J. H.; Balsara, N. P. Predictions of the Thermodynamic Properties of Multicomponent Polyolefin Blends from Measurements on Two-Component Systems. *Macromolecules* **1998**, *31*, 3328−3339.
(95) Jeon, H. S.; Lee, J. H.; Balsara, N. P.; Newstein, M. C. An Experimental Study of the Thermodynamic Properties of Multicomponent Polyolefin Blends with Ordered and Disordered Phases. *Macromolecules* **1998**, *31*, 3340−3352.
(96) Rajasekaran, J. J.; Curro, J. G.; Honeycutt, J. D. Theory for the Phase Behavior of Polyolefin Blends: Application to the Polyethylene/Isotactic Polypropylene Blend. *Macromolecules* **1995**, *28*, 6843−6853.
(97) Teh, J. W.; Rudin, A.; Keung, J. C. A review of polyethylene−polypropylene blends and their compatibilization. *Advances in Polymer Technology* **1994**, *13*, 1−23.
(98) Montes, P.; Rafiq, Y. A.; Hill, M. J. A Study of Blends of Isotactic Polypropylene with High Density Polyethylene by Transmission Electron Microscopy. *Polymer* **1998**, *39*, 6669−6672.
(99) Lo, C.-T.; Seifert, S.; Thiyagarajan, P.; Narasimhan, B. Phase Behavior of Semicrystalline Polymer Blends. *Polymer* **2004**, *45*, 3671−3679.
(100) Kruszynski, J.; Nowicka, W.; Rozanski, A.; Liu, Y.; Parisi, D.; Yang, L.; Pasha, F. A.; Bouyahyi, M.; Jasinska-Walc, L.; Duchateau, R. IPP/HDPE Blends Compatibilized by a Polyester: An Unconventional Concept to Valuable Products. *Sci. Adv.* **2024**, *10* (21), na.
(101) Wu, S. Formation of Dispersed Phase in Incompatible Polymer Blends: Interfacial and Rheological Effects. *Polym. Eng. Sci.* **1987**, *27*, 335−343.
(102) Chaffin, K. A.; Bates, F. S.; Brant, P.; Brown, G. M. Semicrystalline Blends of Polyethylene and Isotactic Polypropylene: Improving Mechanical Performance by Enhancing the Interfacial Structure. *J. Polym. Sci. B Polym. Phys.* **2000**, *38*, 108−121.
(103) Shen, L.; Gorbea, G. D.; Danielson, E.; Cui, S.; Ellison, C. J.; Bates, F. S. Threading-the-Needle: Compatibilization of HDPE/iPP Blends with Butadiene-Derived Polyolefin Block Copolymers. *Proc. Natl. Acad. Sci. U. S. A.* **2023**, *120* (34), No. e2301352120.
(104) Bains, M.; Balke, S. T.; Reck, D.; Horn, J. The Compatibility of Linear Low Density Polyethylene-polypropylene Blends: Viscosity Ratio Plots. *Polym. Eng. Sci.* **1994**, *34*, 1260−1268.
(105) Pérez-Camargo, R. A.; Liu, G.-M.; Wang, D.-J.; Müller, A. J. Experimental and Data Fitting Guidelines for the Determination of Polymer Crystallization Kinetics. *Chin. J. Polym. Sci.* **2022**, *40*, 658−691.
(106) Avrami, M. Granulation, Phase Change, and Microstructure Kinetics of Phase Change. *III. J. Chem. Phys.* **1941**, *9*, 177−184.
(107) Avrami, M. Kinetics of Phase Change 1. *J. Chem. Phys.* **1939**, *7*, 1103.
(108) Hoffman, J. D.; Lauritzen, J. I., Jr Crystallization of Bulk Polymers with Chain Folding: Theory of Growth of Lamellar Spherulites. *J. Res. Natl. Bur Stand A Phys. Chem.* **1961**, *65*, 297.
(109) Lauritzen, J. I., Jr.; Hoffman, J. D. Theory of Formation of Polymer Crystals with Folded Chains in Dilute Solution. *J. Res. Natl. Bur Stand A Phys. Chem.* **1960**, *64*, 73.
(110) Lorenzo, A. T.; Arnal, M. L.; Albuerne, J.; Müller, A. J. DSC Isothermal Polymer Crystallization Kinetics Measurements and the Use of the Avrami Equation to Fit the Data: Guidelines to Avoid Common Problems. *Polym. Test* **2007**, *26*, 222−231.
(111) Hoffman, J. D.; Weeks, J. J. Melting Process and the Equilibrium Melting Temperature of Polychlorotrifluoroethylene. *J. Res. Natl. Bur Stand A Phys. Chem.* **1962**, *66*, 13.
(112) Petraccone, V.; Guerra, G.; De Rosa, C.; Tuzi, A. Extrapolation to the Equilibrium Melting Temperature for Isotactic Polypropylene. *Macromolecules* **1985**, *18*, 813−814.
(113) De Rosa, C.; Guerra, G.; Napolitano, R.; Petraccone, V.; Pirozzi, B. Conditions for the α1-α2 transition in isotactic polypropylene samples. *Eur. Polym. J.* **1984**, *20*, 937−941.
(114) Janimak, J. J.; Cheng, S. Z. D. Crystallization Behavior of Low Molecular Mass Isotactic Poly (Propylene) Fractions. *Polym. Bull.* **1989**, *22*, 95−101.
(115) Cheng, S. Z. D.; Janimak, J. J.; Zhang, A.; Cheng, H. N. Regime Transitions in Fractions of Isotactic Polypropylene. *Macromolecules* **1990**, *23*, 298−303.
(116) Cheng, S. Z. D.; Janimak, J. J.; Zhang, A.; Hsieh, E. T. Isotacticity Effect on Crystallization and Melting in Polypropylene Fractions: 1. Crystalline Structures and Thermodynamic Property Changes. *Polymer* **1991**, *32*, 648−655.
(117) Janimak, J. J.; Cheng, S. Z. D.; Giusti, P. A.; Hsieh, E. T. Isotacticity Effect on Crystallization and Melting in Polypropylene Fractions. II. Linear Crystal Growth Rate and Morphology Study. *Macromolecules* **1991**, *24*, 2253−2260.
(118) Janimak, J. J.; Cheng, S. Z. D.; Zhang, A.; Hsieh, E. T. Isotacticity Effect on Crystallization and Melting in Polypropylene Fractions: 3. *Overall Crystallization and Melting Behavior. Polymer* **1992**, *33*, 728−735.
(119) Mezghani, K.; Phillips, P. J. The γ-Phase of High Molecular Weight Isotactic Polypropylene: III. The Equilibrium Melting Point and the Phase Diagram. *Polymer* **1998**, *39*, 3735−3744.
(120) Yamada, K.; Hikosaka, M.; Toda, A.; Yamazaki, S.; Tagashira, K. Equilibrium Melting Temperature of Isotactic Polypropylene with High Tacticity: 1. *Determination by Differential Scanning Calorimetry. Macromolecules* **2003**, *36*, 4790−4801.
(121) De Rosa, C.; Auriemma, F.; Resconi, L. Influence of Chain Microstructure on the Crystallization Kinetics of Metallocene-Made Isotactic Polypropylene. *Macromolecules* **2005**, *38*, 10080−10088.

https://doi.org/10.1021/acs.macromol.4c01402
Macromolecules 2024, 57, 8748−8762

(122) Clark, E. J.; Hoffman, J. D. Regime III Crystallization in Polypropylene. *Macromolecules* **1984**, *17*, 878−885.
(123) Hoffman, J. D.; Frolen, L. J.; Ross, G. S.; Lauritzen, J. I., Jr. On the Growth Rate of Spherulites and Axialites from the Melt in Polyethylene Fractions: Regime I and Regime II Crystallization. *J. Res. Natl. Bur Stand A Phys. Chem.* **1975**, *79*, 671.

https://doi.org/10.1021/acs.macromol.4c01402
Macromolecules 2024, 57, 8748−8762